

MOL# 87502

## **MONNA, a potent and selective blocker for TMEM16A/Anoctamin-1**

Soo-Jin Oh, Seok Jin Hwang, Jonghoon Jung, Kuai Yu, Jeongyeon Kim, Jung Yoon Choi, H.  
Criss Hartzell, Eun Joo Roh, C. Justin Lee

Center for Neuroscience and Center for Functional Connectomics, Brain Science Institute,  
Korea Institute of Science and Technology (KIST), Seoul, Korea (S-J.O., J.J., J.K., J.Y.C.,  
C.J.L.); Neuroscience Program, University of Science and Technology (UST), Daejeon,  
Korea (C.J.L.); Chemical Kinomics Research Center, Future Convergence Research Division,  
Korea Institute of Science and Technology (KIST), Seoul, Korea (S.J.H., E.J.R.); KU-KIST  
Graduate School of Converging Science and Technology, Seoul, Korea (C.J.L.); and  
Department of Cell Biology, Emory University School of Medicine, Atlanta, Georgia 30322  
USA (K.Y., H.C.H.)

MOL# 87502

## Running title; Potent and selective blockers for ANO1

Address correspondence to:

C. Justin Lee, Center for Neuroscience and Center for Functional Connectomics, Korea  
Institute of Science and Technology, Seoul, Korea 136-791. Tel: +82-2-958-6940; Fax: +82-  
2-958-7219, E-mail: [cjl@kist.re.kr](mailto:cjl@kist.re.kr); and Eun Joo Roh, Chemical Kinomics Research Center,  
Future Convergence Research Division, Korea Institute of Science and Technology (KIST),  
Seoul, Korea 136-791. Tel: +82-2-958-6779; Fax: +82-2-958-5189, E-mail: [r8636@kist.re.kr](mailto:r8636@kist.re.kr)

The number of text pages; 21

The number of tables; 0

The number of figures; 6

The number of references; 23

The number of words in Abstract; 230

The number of words in Introduction; 678

The number of words in Discussion; 988

## ABBREVIATIONS

CaCC, calcium-activated Cl<sup>-</sup> channel; DIDS, 4,4'-diisothiocyanostilbene-2,2'-disulfonic acid;  
DPC, diphenylamine-2-carboxylic acid; <sup>1</sup>H – NMR, Proton nuclear magnetic resonance  
spectroscopy; HR-ESI-MS, high resolution electrospray ionization mass spectrometry;  
MONNA, *N*-((4-methoxy)-2-naphthyl)-5-nitroanthranilic acid; NFA, niflumic acid; NPPB, 5-  
nitro-2-(3-phenylpropylamino) benzoic acid; SAR, structure-activity relationship; TEVC,  
two-electrode voltage-clamp recording; 4TFMPA, *N*-(4-trifluoromethylphenyl)anthranilic  
acid; 4TFP4NA, *N*-(4-trifluorophenyl)-4-nitroanthranilic acid

MOL# 87502

## Abstract

TMEM16A/Anoctamin-1 (ANO1) is a protein widely expressed in mammalian tissues and has the properties of the classical calcium-activated chloride channel (CaCC). This protein has been implicated in numerous major physiological functions. However, the lack of effective and selective blockers has hindered a detailed study of the physiological functions of this channel. In this study, we have developed a potent and selective blocker for endogenous ANO1 in *Xenopus laevis* oocytes (xANO1) using a drug screening method we had previously established (Oh et al., 2008). We have synthesized a number of anthranilic acid derivatives and have determined the correlation between biological activity and the nature and position of substituents in these derived compounds. A structure-activity relationship (SAR) revealed novel chemical classes of xANO1 blockers. The derivatives contain a -NO<sub>2</sub> group on position 5 of a naphthyl group substituted anthranilic acid, and they fully blocked xANO1 chloride currents with an IC<sub>50</sub> < 10 μM. The most potent blocker, *N*-((4-methoxy)-2-naphthyl)-5-nitroanthranilic acid (MONNA) had an IC<sub>50</sub> of 0.08 μM for xANO1. Selectivity tests revealed that other chloride channels such as bestrophin-1, CLC2 and cystic fibrosis transmembrane conductance regulator (CFTR) were not appreciably blocked by 10 ~ 30 μM MONNA. The potent and selective blockers for ANO1 identified here should permit pharmacological dissection of ANO1/CaCC function and serve as potential candidates for drug therapy of related diseases such as hypertension, cystic fibrosis, bronchitis, asthma and hyperalgesia.

MOL# 87502

## Introduction

Calcium-activated chloride channels (CaCCs) have been found in a wide range of organisms and tissues. They have fundamental and wide-ranging physiological roles in functions such as epithelial secretion, sensory transduction and adaptation, nociception, regulation of smooth muscle cell contraction and vascular tone, and the control of neuronal and cardiac excitability (Hartzell et al., 2005). Therefore, CaCCs are potential drug targets for diarrhea, asthma, cystic fibrosis, and hypertension (Verkman and Galletta, 2009). CaCCs were first described in the early 1980s, in *Xenopus laevis* oocytes, where they generate the fertilization potential that generates a fast electrical inhibition to prevent polyspermy (Barish, 1983; Miledi, 1982). However, the molecular identity of these channels remained elusive until the transmembrane protein with unknown function 16 (TMEM16A)/anoctamin-1 (ANO1) was identified as a CaCC in 2008 (Caputo et al., 2008; Schroeder et al., 2008; Yang et al., 2008). Since then, ANO1 has rapidly garnered attention and a number of reports have described the properties and physiological roles of this protein (Huang et al., 2009). Notably, a recent study revealed that ANO1 acts as a heat sensor to detect nociceptive thermal stimuli in sensory neurons and possibly mediate nociception (Cho et al., 2012).

The anoctamin family consists of ten different protein subtypes. Among them, ANO1 has been the most extensively studied (Huang et al., 2009). ANO1 has very similar properties to endogenous CaCCs that have been observed in many different cells, tissues and organisms. These properties include low field-strength anion selectivity,  $\text{Ca}^{2+}$  sensitivity, voltage dependence and pharmacological profile. Despite the physiological importance of ANO1, the lack of a potent and selective blocker for this protein has impeded a better understanding of the channel at the molecular, biophysical and pharmacological level. Currently available blockers for CaCCs, including ANO1, include niflumic acid (NFA), 4,4'-diisothiocyanostilbene-2,2'-disulfonic acid (DIDS), 5-nitro-2-(3-phenylpropylamino) benzoic

MOL# 87502

acid (NPPB) and mefloquine, all of which must be applied at high concentrations to completely block ANO1. The half-maximal concentration for inhibition ( $IC_{50}$ ) of NFA, DIDS and NPPB are reported to be 37.3  $\mu$ M, 10.7  $\mu$ M and 32.3  $\mu$ M, respectively (Oh et al., 2008). Furthermore, these blockers are known to cause undesirable side effects and to block other channels. For example, NFA and DIDS also block the volume-regulated anion channel (VRAC) in some cell types (Greenwood and Large, 1998; Xu et al., 1997), while all three, NFA, DIDS and NPPB, have a blocking effect on the  $K^+$  channel current (Greenwood and Leblanc, 2007; Wang et al., 1997). In addition, NFA, DIDS and NPPB cause an elevation of intracellular  $Ca^{2+}$  concentration in several cell types, which can elicit other cellular responses (Reinsprecht et al., 1995; Schultheiss et al., 2000; Shaw et al., 1995). More recently, several ANO1 inhibitors, such as dichlorophen, benzbromarone and hexachlorophene have been identified with high-throughput screening methods, having an  $IC_{50}$  of 5.49  $\mu$ M, 9.97  $\mu$ M, and 10.0  $\mu$ M, respectively (Huang et al., 2012). These compounds showed somewhat improved potency over conventional blockers but still fell short of submicromolar potency. In another high-throughput screening study, an aminophenylthiazole (T16A<sub>inh</sub>-A01, (Namkung et al., 2011)) was found to have an  $IC_{50}$  of around 1  $\mu$ M, but no selectivity information was available. Thus, because of these issues related to low potency and selectivity, there is a very pressing need for improved ANO1 blockers.

Many attempts have been made to uncover chemical compounds that block the endogenous CaCC in *Xenopus laevis* oocytes. In a previous study, we established an optimized protocol for large-scale drug screening using a two-electrode voltage-clamp recording (TEVC) system to search for better blockers for endogenous CaCCs in *Xenopus laevis* oocytes (Oh et al., 2008), which were revealed to be dominantly mediated by endogenous xANO1 (Yang et al., 2008). In our previous study, we found a structural similarity between commercially available CaCC blockers and *N*-(4-

MOL# 87502

trifluoromethylphenyl)anthranilic acid (4TFMPA), a novel potent blocker for xANO1, with an  $IC_{50}$  of 6.0  $\mu$ M, which was synthesized based on SAR analysis. In the present study, using the same screening method, we further examined the blocking effect of synthesized compounds using an in-depth SAR analysis to discover new ANO1 blockers that have an  $IC_{50}$  of less than 1  $\mu$ M.

## Materials and Methods

**Preparation of oocytes:** As described previously (Oh et al., 2008), mature stage V–VI oocytes were harvested from adult *Xenopus laevis* females (Xenopus-I Inc, Dexter, Michigan, USA) that were maintained in an automated maintenance system, Xenopus System (Aquatic Habitats, Apopka, Florida, USA). All experimental procedures described below were performed in accordance with KIST (Seoul, Korea) institutional guidelines for humane animal handling. Animals were anaesthetized by cooling with ice. Surgically removed ovarian follicles were treated with 2 mg/ml collagenase type IA at room temperature for 90 min in  $Ca^{2+}$ -free Barth's solution containing: 89 mM NaCl, 1.0 mM KCl, 2.4 mM  $NaHCO_3$ , 0.82 mM  $MgSO_4$  and 10 mM HEPES (pH 7.4). Oocytes were extensively rinsed with normal Barth's solution containing: 88 mM NaCl, 1.0 mM KCl, 2.4 mM  $NaHCO_3$ , 0.82 mM  $MgSO_4$ , 0.33 mM  $Ca(NO_3)_2$ , 1.41 mM  $CaCl_2$  and 5 mM HEPES (pH 7.4), placed in a culture of Barth's solution containing: 88 mM NaCl, 1.0 mM KCl, 2.4 mM  $NaHCO_3$ , 0.82 mM  $MgSO_4$ , 0.33 mM  $Ca(NO_3)_2$ , 0.91 mM  $CaCl_2$ , 10 mM HEPES, 10  $\mu$ g/ml streptomycin and 10  $\mu$ g/ml penicillin (pH 7.4), and maintained at 18 °C. Oocytes were used 1 ~ 4 days after isolation.

**Synthesis:** Some anthranilic acid derivatives (4f and six compounds that are not designated in Fig. 2F) had been previously synthesized and reported by us (Oh et al., 2008). The other anthranilic acid derivatives were synthesized as described in Fig.1. Step A. II, IV and VIII: Thionyl chloride was added dropwise to a solution of benzoic acid derivative (I, III,

MOL# 87502

and VII) in anhydrous methyl alcohol at 0 °C. After this addition, the mixture was stirred at reflux for 8 ~ 12 hrs. The reaction mixture was basified with 10 % sodium bicarbonate and ethyl acetate was added. The organic layer was dried over anhydrous MgSO<sub>4</sub>, filtered and the solvent was evaporated to give the products II, IV and VIII. Step B. IX: Triflic anhydride was added dropwise to a solution of 4-trifluoromethyl-2-hydroxybenzoic acid methyl ester (VIII) in pyridine and dichloromethane (DCM). This was stirred at room temperature for 6 hrs and acidified by the addition of 1 N HCl (aq). The mixture was extracted with DCM and washed with brine. The organic layer was dried over anhydrous MgSO<sub>4</sub>, filtered and the solvent was evaporated. IX was purified by column chromatography. Amine derivatives (2a-q, Supplemental methods, Compound synthesis 2) were prepared by this method, except for the commercially available amines. Step C. V and X: Buchward-Hartwig cross coupling of amine (2a-q, IV) and bromo (1b, II) [or triflate (1a, IX)] gave anthanilic acid methyl ester (V, X). Tris (dibenzylideneacetone) dipalladium (0)-chloroform adduct (0.05 eq) and (±)-2,2'-bis (diphenylphosphino)-1,1'-binaphthalene (0.10 eq) in anhydrous toluene (3 ml) were stirred at room temperature for 30 min. Then, 2-bromo-*N*-nitrobenzoic acid methyl ester, Cs<sub>2</sub>CO<sub>3</sub> (1.4 eq) and aniline derivative (1.2 eq) were added and stirred at 110 ~ 130 °C for 5 ~ 10 hrs. The reaction mixture was filtered through Celite and concentrated *in vacuo*. Anthanilic acid methyl ester (V, X) was purified by column chromatography. Step D. VI: Iodination of bromo (V) gave VI. V, NaI (2 eq), CuI (0.05 eq) and trans-*N,N'*-dimethylcyclohexane-1,2-diamine (0.1 eq) in 1,4-dioxane were stirred at 110 °C for 5 days. The reaction mixture was filtered through Celite and concentrated *in vacuo*. VI was purified by column chromatography. Step E. 3, 4, 5, 6: Hydrolysis of benzoic acid methyl ester derivative (V, VI and X) was accomplished by refluxing tetrahydrofuran (THF) / methanol (MeOH) / H<sub>2</sub>O (5 : 3 : 2) solution in the presence of lithium hydroxide. The reaction mixture was acidified by the addition of 1N HCl (aq) then extracted with ethyl acetate and washed with brine. The organic

MOL# 87502

layer was dried over anhydrous  $\text{MgSO}_4$ , filtered and the solvent was evaporated to give anthranilic acid derivatives (3, 4, 5 and 6, Supplemental methods, Compound synthesis 1).

### Representative examples of active compounds

***N*-((3-methoxy)naphthyl)-5-nitroanthranilic acid (5p)** The final step yields 94.6 % (orange solid). Proton nuclear magnetic resonance spectroscopy ( $^1\text{H}$  - NMR, 400 MHz, Dimethyl sulfoxide ( $\text{DMSO}$ ) -  $d_6$ )  $\delta$  10.64 (bs, 1H), 8.97 (d,  $J$  = 2.7 Hz, 1H), 8.06 (dd,  $J$  = 9.4, 2.6 Hz, 1H), 7.84 (d,  $J$  = 8.7 Hz, 1H), 7.82 (d,  $J$  = 9.3 Hz, 1H), 7.53-7.49 (m, 1H), 7.39-7.35 (m, 1H), 7.19 (d,  $J$  = 1.9 Hz, 1H), 7.15 (d,  $J$  = 2.3 Hz, 1H), 6.82 (d,  $J$  = 9.5 Hz, 1H), 3.91 (s, 3H);  $^{13}\text{C}$  - NMR (100 MHz,  $\text{DMSO}$  -  $d_6$ )  $\delta$  169.4, 157.5, 154.0, 137.0, 135.8, 129.9, 128.9, 127.7, 125.0, 122.4, 115.7, 114.2, 111.4, 106.0, 55.9; high resolution electrospray ionization mass spectrometry (HR-ESI-MS)  $m/z$  337.0838  $[\text{M} - \text{H}]^-$ . ***N*-((6-methoxy)naphthyl)-5-nitroanthranilic acid (5r)** The final step yields 90.1 % (yellow solid).  $^1\text{H}$  - NMR (400 MHz,  $\text{DMSO}$  -  $d_6$ )  $\delta$  10.65 (bs, 1H), 8.75 (d,  $J$  = 2.8 Hz, 1H), 8.09 (dd,  $J$  = 9.4, 2.8 Hz, 1H), 7.84 (d,  $J$  = 8.0 Hz, 1H), 7.78 (d,  $J$  = 9.2 Hz, 1H), 7.56 (dd,  $J$  = 7.8, 7.6 Hz, 1H), 7.46 (s, 1H), 7.41 (d,  $J$  = 7.2 Hz, 1H), 7.22 (dd,  $J$  = 9.0, 2.4 Hz, 1H), 6.66 (d,  $J$  = 9.6 Hz, 1H), 3.90 (s, 3H);  $^{13}\text{C}$  - NMR (100 MHz,  $\text{DMSO}$  -  $d_6$ )  $\delta$  169.4, 158.2, 154.3, 143.5, 136.8, 136.4, 134.5, 129.8, 128.9, 127.2, 126.6, 124.9, 121.3, 120.0, 113.9, 111.2, 107.3, 55.8; HR-ESI-MS  $m/z$  337.0823  $[\text{M} - \text{H}]^-$ . ***N*-((4-methoxy)-2-naphthyl)-5-nitroanthranilic acid (5v)** The final step yields 98.0 % (orange solid).  $^1\text{H}$  - NMR (400 MHz,  $\text{DMSO}$  -  $d_6$ )  $\delta$  10.54 (bs, 1H), 8.74 (d,  $J$  = 2.6 Hz, 1H), 8.19 (dd,  $J$  = 9.4, 2.5 Hz 1H), 8.11 (d,  $J$  = 8.2 Hz, 1H), 7.84 (d,  $J$  = 8.0 Hz, 1H), 7.56-7.45 (m, 3H), 7.35 (d,  $J$  = 9.4 Hz, 1H), 6.95 (d,  $J$  = 9.5 Hz, 1H);  $^{13}\text{C}$  - NMR (100 MHz,  $\text{DMSO}$  -  $d_6$ )  $\delta$  169.2, 156.6, 152.7, 137.2, 136.7, 134.7, 129.8, 128.9, 127.8, 127.7, 125.5, 123.5, 122.0, 114.4, 113.2, 111.8, 102.8, 56.4; HR-ESI-MS  $m/z$  337.0831  $[\text{M} - \text{H}]^-$ . ***N*-((7-methoxy)-2-naphthyl)-5-nitroanthranilic acid (5y)** The final step yields 94.9 % (yellow solid).  $^1\text{H}$  - NMR (400 MHz,  $\text{DMSO}$  -  $d_6$ )  $\delta$  10.55 (bs, 1H), 8.73 (d,  $J$  = 2.8 Hz, 1H), 8.19 (dd,  $J$  = 9.4,



MOL# 87502

2.8 Hz, 1H), 7.91 (d,  $J$  = 8.6 Hz, 1H), 7.83 (d,  $J$  = 9.0 Hz, 1H), 7.78 (d,  $J$  = 1.3 Hz, 1H), 7.32-7.29 (m, 2H), 7.28 (d,  $J$  = 9.4 Hz, 1H), 7.14 (dd,  $J$  = 8.9, 2.4 Hz, 1H), 3.87(s, 3H));  $^{13}\text{C}$  - NMR (100 MHz, DMSO -  $d_6$ )  $\delta$  169.2, 158.4, 152.7, 137.2, 136.8, 135.6, 129.8, 129.7, 128.9, 126.8, 121.1, 120.0, 118.7, 114.1, 111.7, 106.2, 55.7; HR-ESI-MS  $m/z$  337.0830  $[\text{M} - \text{H}]^-$ . ***N*-((8-methoxy)-2-naphthyl)-5-nitroanthranilic acid (5z)** The final step yields 91.1 % (yellow solid).  $^1\text{H}$  - NMR (400 MHz, DMSO -  $d_6$ ) 10.56 (bs, 1H), 8.74 (d,  $J$  = 2.6 Hz, 1H), 8.20 (dd,  $J$  = 9.4, 2.6 Hz, 1H), 8.03 (s, 1H), 7.98 (d,  $J$  = 8.6 Hz, 1H), 7.51 (d,  $J$  = 8.5 Hz, 1H), 7.43 (dd,  $J$  = 7.7, 7.7 Hz, 1H), 7.22 (d,  $J$  = 9.4 Hz, 1H), 7.01 (d,  $J$  = 7.5 Hz, 1H), 3.97 (s, 3H);  $^{13}\text{C}$  - NMR (100 MHz, DMSO -  $d_6$ )  $\delta$  169.1, 154.8, 152.8, 137.2, 135.8, 132.4, 129.9, 129.8, 128.9, 126.5, 125.8, 124.1, 120.3, 115.3, 113.7, 111.7, 105.6, 56.1; HR-ESI-MS  $m/z$  337.0833  $[\text{M} - \text{H}]^-$ . ***N*-((4-bromo)naphthyl)-5-nitroanthranilic acid (5ab)** The final step yields 97.6 % (brown solid).  $^1\text{H}$  - NMR (400 MHz, DMSO -  $d_6$ )  $\delta$  10.72 (bs, 1H), 8.77 (d,  $J$  = 2.7 Hz, 1H), 8.24 (d,  $J$  = 8.4 Hz, 1H), 8.09 (dd,  $J$  = 9.4, 2.8 Hz, 1H), 8.00-7.97 (m, 2H), 7.79 (dd,  $J$  = 7.7, 7.3 Hz, 1H), 7.70 (dd,  $J$  = 7.7, 7.2 Hz, 1H), 7.55 (d,  $J$  = 8.0 Hz, 1H), 6.72 (d,  $J$  = 9.4 Hz, 1H);  $^{13}\text{C}$  - NMR (100 MHz, DMSO -  $d_6$ )  $\delta$  169.3, 153.9, 137.2, 135.0, 132.6, 130.9, 130.6, 129.7, 129.0, 128.8, 128.5, 127.7, 124.4, 123.4, 120.5, 114.1, 111.7; HR-ESI-MS  $m/z$  384.9819  $[\text{M} - \text{H}]^-$ . ***N*-((4-bromo)-2-naphthyl)-5-nitroanthranilic acid (5ac)** The final step yields 93.5 % (yellow solid).  $^1\text{H}$  - NMR (400 MHz, DMSO -  $d_6$ )  $\delta$  10.51 (bs, 1H), 8.74 (s, 1H), 8.22 (d,  $J$  = 9.8 Hz, 1H), 8.11 (d,  $J$  = 8.0 Hz, 1H), 8.00-7.93 (m, 3H), 7.66-7.64 (m, 2H), 7.30 (d,  $J$  = 8.8 Hz, 1H);  $^{13}\text{C}$  - NMR (100 MHz, DMSO -  $d_6$ )  $\delta$  168.9, 152.2, 137.7, 136.8, 134.9, 129.8, 129.5, 128.7, 128.2, 127.9, 127.6, 126.6, 123.1, 121.3, 114.4; HR-ESI-MS  $m/z$  384.9839  $[\text{M} - \text{H}]^-$ . ***N*-((7-bromo)-2-naphthyl)-5-nitroanthranilic acid (5ad)** The final step yields 85 % (yellow solid).  $^1\text{H}$  - NMR (400 MHz, DMSO -  $d_6$ )  $\delta$  10.64 (bs, 1H), 8.73 (d,  $J$  = 2.7, Hz, 1H), 8.20-8.17 (m, 2H), 8.01 (d,  $J$  = 8.6 Hz, 1H), 7.89 (d,  $J$  = 8.2 Hz, 2H), 7.60-7.58 (m, 1H), 7.53 (dd,  $J$  = 8.6, 1.8 Hz, 1H), 7.33 (d,  $J$  = 9.4 Hz, 1H);  $^{13}\text{C}$  - NMR (100 MHz, DMSO -  $d_6$ )  $\delta$

MOL# 87502

169.1, 152.0, 137.5, 135.3, 130.3, 130.0, 129.6, 128.8, 123.9, 120.6, 119.2, 114.0, 112.2; HR-ESI-MS  $m/z$  334.9822  $[M - H]^-$ . ***N*-((8-bromo)-2-naphthyl)-5-nitroanthranilic acid (5ae)**

The final step yields 92.4 % (yellow solid).  $^1H$  - NMR (400 MHz, DMSO -  $d_6$ )  $\delta$  10.69 (bs, 1H), 8.75 (d,  $J = 2.8$  Hz, 1H), 8.22 (dd,  $J = 9.4, 2.8$  Hz, 1H), 8.09 (d,  $J = 8.8$  Hz, 1H), 8.03 (s, 1H), 8.00 (d,  $J = 8.2$  Hz, 1H), 7.90 (d,  $J = 7.4$  Hz, 1H), 7.62 (dd,  $J = 8.7, 1.9$  Hz, 1H), 7.42 (d,  $J = 7.8, 7.8$  Hz, 1H), 7.33 (d,  $J = 9.4$  Hz, 1H);  $^{13}C$  - NMR (100 MHz, DMSO -  $d_6$ )  $\delta$  169.0, 152.1, 138.4, 137.7, 132.5, 132.4, 131.3, 131.0, 129.7, 128.8, 128.6, 126.7, 124.5, 121.4, 119.0, 114.1, 112.6; HR-ESI-MS  $m/z$  384.9837  $[M - H]^-$ . ***N*-((4-iodo)naphthyl)-5-nitroanthranilic acid (5af)** The final step yields 83.3 % (yellow solid).  $^1H$  - NMR (400 MHz, DMSO -  $d_6$ )  $\delta$  10.70 (bs, 1H), 8.76 (s, 1H), 8.22 (d,  $J = 7.7$  Hz, 1H), 8.09 (dd,  $J = 8.0, 7.7$  Hz, 2H), 7.91 (d,  $J = 8.2$  Hz, 1H), 7.74 (dd,  $J = 7.6, 6.9$  Hz, 1H), 7.65 (dd,  $J = 7.3, 7.2$  Hz, 1H), 7.39 (d,  $J = 7.7$  Hz, 1H), 6.72 (d,  $J = 9.3$  Hz, 1H);  $^{13}C$  - NMR (100 MHz, DMSO -  $d_6$ )  $\delta$  169.3, 153.9, 137.9, 137.2, 135.9, 135.2, 132.8, 130.5, 129.7, 129.3, 128.8, 128.5, 124.9, 123.4, 114.2, 111.8, 98.1; HR-ESI-MS  $m/z$  432.9682  $[M - H]^-$ . ***N*-((4-iodo)-2-naphthyl)-5-nitroanthranilic acid (5ag)** The final step yields 95.3 % (yellow solid).  $^1H$  - NMR (400 MHz, DMSO -  $d_6$ )  $\delta$  10.53 (bs, 1H), 8.74 (bs, 1H), 8.21 (d,  $J = 8.0$  Hz, 1H), 8.13 (bs, 1H), 8.00 (bs, 2H), 7.91 (d,  $J = 5.9$  Hz, 1H), 7.62 (bs, 2H), 7.28 (d,  $J = 8.8$  Hz, 1H);  $^{13}C$  - NMR (100 MHz, DMSO -  $d_6$ )  $\delta$  169.0, 152.4, 137.6, 137.1, 134.9, 134.7, 134.2, 132.2, 131.6, 129.8, 128.9, 128.8, 128.2, 114.4, 112.4, 101.1; HR-ESI-MS  $m/z$  432.9653  $[M - H]^-$ . ***N*-((7-iodo)-2-naphthyl)-5-nitroanthranilic acid (5ah)** The final step yields 96.2 % (yellow solid).  $^1H$  - NMR (400 MHz, DMSO -  $d_6$ )  $\delta$  10.93 (bs, 1H), 8.75 (bs, 1H), 8.37 (bs, 1H), 8.18 (d,  $J = 6.7$  Hz, 1H), 7.99 (d,  $J = 8.5$  Hz, 1H), 7.86 (bs, 1H), 7.74 (bs, 2H), 7.51 (d,  $J = 8.0$  Hz, 1H), 7.34 (d,  $J = 8.6$  Hz, 1H);  $^{13}C$  - NMR (100 MHz, DMSO -  $d_6$ )  $\delta$  169.1, 152.2, 137.5, 137.2, 136.1, 135.8, 134.2, 130.1, 130.0, 129.9, 128.8, 124.2, 119.3, 114.2, 112.4, 93.8; HR-ESI-MS  $m/z$  432.9686  $[M - H]^-$ .  $^1H$  and  $^{13}C$  - NMR spectra were recorded either on a spectrometer

MOL# 87502

operating at Bruker (Billerica, Massachusetts, USA) 400 and 100 MHz, respectively. HR-ESI-MS was carried out by the Advanced Analysis Center at Korea Institute of Science and Technology.

### **Electrophysiology of *Xenopus laevis* oocytes**

In order to test the blocking effect of compounds on xANO1, xANO1 was activated by permeabilizing the plasma membrane to  $\text{Ca}^{2+}$  and changing the extracellular  $\text{Ca}^{2+}$  concentration. The oocyte plasma membrane was made permeable to  $\text{Ca}^{2+}$  by treatment with the  $\text{Ca}^{2+}$  ionophore, ionomycin.  $\text{Ca}^{2+}$  sequestration by intracellular stores was inhibited with thapsigargin. Oocytes were incubated in an oocyte recording solution containing 96 mM NaCl, 2 mM KCl, 2 mM  $\text{MgCl}_2$ , 0.5 mM EGTA and 10 mM HEPES (pH 7.4), that also contained 10  $\mu\text{M}$  ionomycin, for a 30 min period. After 30 min, the ionomycin was removed from the external solution by washing with oocyte recording solution. Ionomycin-treated oocytes were subsequently incubated in the oocyte recording solution containing 1  $\mu\text{M}$  thapsigargin for 90 min. Thapsigargin was then also removed by washing with the oocyte recording solution. Two-electrode voltage-clamp recordings were made using the Warner model OC725B two-electrode voltage clamp amplifier (Warner Instruments, Inc., Hamden, CT, USA) with 1 M KCl-filled microelectrodes (WPI; Sarasota, FL; 1B150F-4) pulled with a P-97 programmable pipette puller (Sutter Instrument Co., Novato, CA, USA). Microelectrodes had resistances of 1 ~ 3 M $\Omega$ . During recordings, oocytes were continuously perfused with oocyte recording solution. All recordings were obtained at a holding potential of -60 mV. Synthesized drug derivatives were prepared in separate bottles and applied by gravity. The flow of solutions was approximately 1 ml/min.

### **Electrophysiology of cultured astrocytes, HEK293 cells**

Mouse astrocyte cell cultures were prepared as previously described (Park et al., 2009). HEK293 cells were transfected with cDNA (hANO1 or mANO1 or mCIC2) expression

MOL# 87502

plasmids tagged with EGFP, using Effectene (Qiagen, Valencia, CA, USA) or a blend of lipids (Fugene-6; Roche Molecular Biochemicals, Indianapolis, IN) at 1  $\mu$ g of DNA per 35-mm culture dish. Single cells identified by green fluorescent protein (EGFP) fluorescence were used for whole-cell patch clamp experiments within 72 hours. Transfected HEK293 cells were recorded using a conventional whole-cell and an excised inside-out patch-clamp. Fire-polished borosilicate glass patch pipettes were 3 ~ 5 M $\Omega$ . Experiments were conducted at room temperature (20 ~ 25 °C). To activate the channels directly, cultured astrocytes or HEK293 cells were patch clamped with a high Ca<sup>2+</sup> intracellular solution that contained: 146 mM CsCl, 5 mM (Ca<sup>2+</sup>)-EGTA-N-methyl-D-glucamine (NMDG), 2 mM MgCl<sub>2</sub>, 8 mM HEPES, and 10 mM sucrose, at pH 7.3, adjusted with NMDG. The free Ca<sup>2+</sup> concentration was estimated to be 4.5  $\mu$ M (Hartzell et al., 2005). The extracellular solution contained the following: 150 mM NaCl, 10 mM HEPES, 3 mM KCl, 2 mM CaCl<sub>2</sub>, 2 mM MgCl<sub>2</sub>, and 5.5 mM glucose or 140 mM NaCl, 5 mM KCl, 2 mM CaCl<sub>2</sub>, 1 mM MgCl<sub>2</sub>, 15 mM glucose, 10 mM HEPES at pH 7.3 adjusted with NaOH (300 ~ 320 mOsm). Current-voltage curves were established by applying 500 ms duration voltage ramps from -100 to +100 mV. Data were acquired with an Axopatch 200A amplifier controlled by Clampex 10.0 software via a Digidata 1322A data acquisition system (Molecular Devices, Sunnyvale, CA, USA). mBest1 current or hANO1 current was recorded after treatment with MONNA for 10 minutes. Cells were ruptured and calcium-induced currents were recorded in the presence of MONNA. Current amplitude at one time point of 100 ~ 300 second after rupture was selected to be analyzed.

### Chemicals

Chemical compounds, including the following reagents, were purchased from Sigma-Aldrich Co. (St. Louis, MO, USA); collagenase type 1A, ionomycin-Ca<sup>2+</sup> salt and

MOL# 87502

thapsigargin, chelerythrine. HEPES (4-(2-hydroxyethyl)-1-piperazineethanesulfonic acid) was obtained from J.T.Baker<sup>®</sup> (Mallinckrodt Baker Inc., Phillipsburg, NJ, USA).

### **Data analysis**

Currents were digitally recorded with AxoScope software (Axon Instruments, Burlingame, CA, USA) and Clampex 10.0 software. Data analysis was performed with SigmaPlot 10.0 (Systat Software Inc., San Jose, CA, USA). All current responses elicited during application of a blocker were normalized to the average of a  $\text{Ca}^{2+}$ -induced  $\text{Cl}^-$  current applied before application of the blocker. Normalized and average data were fitted using the SigmaPlot three parameter logistic function in order to determine the dose-response relationship and the  $\text{IC}_{50}$ . All data are expressed as mean  $\pm$  standard error of the mean. Statistical analyses were performed using a 2-tailed t-test.

### **Results**

#### **Potency of synthesized derivatives with a phenyl group at the B position.**

Synthesis of anthranilic acid derivatives was accomplished as described in Fig. 1 (See Materials and Methods and Supplemental methods). Synthesized and purified compounds were tested for their blocking ability on xANO1 in  $\text{Ca}^{2+}$  ionophore-treated oocytes using the TEVC technique as described previously (Oh et al., 2008). We already showed that two repetitive calcium treatments induced currents with almost same amplitude in our screening system (Oh et al., 2008). We confirmed that 4-repetitive calcium treatments induce stable currents with similar average amplitude and small variation (Fig. 2A,B). We expanded our well-established recording method to permit simultaneous recording from four oocytes (Fig. 2C). A control ANO1 current in the oocyte was recorded by first adding 5 mM  $\text{Ca}^{2+}$  to the external bath for 5 s.  $\text{Ca}^{2+}$  was then removed and the drug derivatives added to the zero- $\text{Ca}^{2+}$  solution before  $\text{Ca}^{2+}$  was added to activate ANO1. Current traces were recorded using the 4-

MOL# 87502

channel recording system. There was a small variation in peak current amplitudes. In response to repetitive 5 s applications of 5 mM  $\text{Ca}^{2+}$  plus treatment with the synthesized compound over the concentration range (1  $\mu\text{M}$  ~ 300  $\mu\text{M}$ ), peak amplitudes revealed a concentration-dependent block of the xANO1 current and values for  $\text{IC}_{50}$  were obtained from dose-response curves. Representative dose-response relation of *N*-(4-trifluorophenyl)-4-nitroanthranilic acid (4TFP4NA) block of xANO1 currents is shown in Fig. 2D.

As we have previously shown that anthranilic acid derivatives with a *para*-substituted phenyl ring showed the highest blocking potency (Oh et al., 2008), we synthesized various anthranilic acid derivatives with *para*-positioned substituent groups on the phenyl ring (at position B in Fig. 2E) and with nitro ( $-\text{NO}_2$ ) groups positioned at different locations on the benzoic acid ring (at positions A1-A3 in Fig. 2E). Fig. 2F gives the  $\text{IC}_{50}$  values of test compounds. Derivative compounds having  $-\text{NO}_2$  positioned at A2 on the benzoic acid ring had a relatively high potency in all groups. Substituting different halogen groups on the phenyl ring (position B in Fig. 2E), revealed that potency increased with increasing size of the halogen ( $\text{I} > \text{Br} > \text{Cl} > \text{F}$ ). For substituents with a trifluoromethyl group ( $-\text{CF}_3$ ),  $-\text{NO}_2$  or methoxy group ( $-\text{OCH}_3$ ) on the phenyl ring, the most hydrophobic, that with  $-\text{CF}_3$  was the most potent.

**Different positional effect was observed in derivatives with phenyl or naphthyl groups at the B position.**

As shown in Fig. 2F, the compounds with greatest potency were produced when  $-\text{NO}_2$  was located at position A2 on the benzoic acid ring. We have already verified that 4TFMPA with a  $-\text{CF}_3$  group *para*-positioned on the phenyl ring, produced a better blocking effect compared to *N*-(4-nitrophenyl)anthranilic acid having a  $-\text{NO}_2$  group located at the same position. Fig. 2F shows that the derivative compound having  $-\text{CF}_3$  on the phenyl ring had a higher potency than the derivative having  $-\text{NO}_2$  on the phenyl ring. Therefore, we replaced

MOL# 87502

the -NO<sub>2</sub> substituent group with -CF<sub>3</sub> at position A2 on the benzoic acid ring (Fig. 3A). However, we found that derivative compounds with -NO<sub>2</sub> located at position A2 on the benzoic acid ring were much more potent than compounds with -CF<sub>3</sub> at the same position (Fig. 3B).

Since compounds with more hydrophobic substituent groups had a higher potency in Fig. 2F, we further investigated additional derivative compounds possessing the more hydrophobic naphthyl group at position B (Fig. 3A) in combination with the benzoic acid ring. We synthesized a series of anthranilic acid derivatives having the *N*- $\alpha$ -naphthyl group. As expected, compounds with a naphthyl group were more potent than compounds with a phenyl group. In contrast to compounds containing the phenyl group, compounds with -NO<sub>2</sub> at position A1 of the benzoic acid ring possessing the naphthyl group were demonstrated to be substantially potent blockers compared to compounds with -NO<sub>2</sub> at the A2 position (Fig. 3C). These data support the idea that a close correlation exists between the potency of blocking xANO1 and the position of substituents on the benzoic acid ring or the hydrophobicity of substituents.

#### **Effect of substituent position in the naphthyl group on blocking potency**

As depicted in Fig. 3C, higher potency was observed for derivatives with 4-iodo, 4-bromo and 4-methoxy substituents on the *N*- $\alpha$ -naphthyl group. To evaluate the positional effect, all positions on the naphthyl group (Fig. 4A) were substituted with a -OCH<sub>3</sub> group. Because it was easier to synthesize derivatives with -OCH<sub>3</sub> than with iodine (-I), we prepared various compounds with -OCH<sub>3</sub> at different positions. Fig. 4B shows that all tested compounds conferred a relatively high potency that fully blocked the xANO1 chloride current with an IC<sub>50</sub> < 10  $\mu$ M. We further synthesized anthranilic acid derivatives with  $\beta$ -naphthyl containing -OCH<sub>3</sub> at different positions (Fig. 4C) and examined the blocking effect of these compounds for xANO1 (Fig. 4D). We also synthesized compounds that had bromine

MOL# 87502

(-Br) and -I substituents at positions C3, C10, C13 or C14 (Fig. 4E). These positions were selected because they showed a relatively higher potency with -OCH<sub>3</sub>. We discovered that anthranilic acid derivatives with the  $\beta$ -naphthyl group with -OCH<sub>3</sub> at position C10, with -I at C10, -Br at C13, and -I at C13 had a profound blocking effect on xANO1, with an IC<sub>50</sub> of 0.08 $\mu$ M, 0.90 $\mu$ M, 0.22 $\mu$ M and 0.55 $\mu$ M respectively (Fig. 4E). The most potent blocker found, an anthranilic derivative having  $\beta$ -naphthyl with a -OCH<sub>3</sub> group at position C10 (*N*-((4-MethOxy)-2-Naphthyl)-5-Nitroanthranilic Acid) and with an IC<sub>50</sub> of 0.08 $\mu$ M, we named MONNA.

### Validation of potent blocker MONNA on the steady-state current

In the blocker screening protocol, oocytes were treated with ionomycin to permeabilize the membrane to allow Ca<sup>2+</sup> influx to activate xANO1. It is possible that the apparent blocking effect could be due to a direct block of ionomycin-mediated Ca<sup>2+</sup> influx. To confirm that the prominent blocking effect of MONNA occurs at the ionophore or xANO1, we investigated the effect of MONNA on Ba<sup>2+</sup>- induced currents carried by the ionophore (Fig. 5A). In response to application of Ba<sup>2+</sup>, a small current mediated by ionomycin was produced. This current was not blocked by MONNA nor by 4TFMPA (Fig. 5B).

In our previous study, we showed that Cl<sup>-</sup> currents elicited by Ca<sup>2+</sup> influx in oocytes permeabilized with ionomycin consisted of a fast peak and a slow steady-state component (Oh et al., 2008). In addition, Schroeder et al., demonstrated that recording from ionomycin-treated *Axolotl* oocytes injected with xANO1 cRNA had calcium-activated currents with both fast and slow components (Schroeder et al., 2008), indicating that both components are mediated by xANO1. To examine whether tested blockers inhibit both the slow steady current as well as the fast current, we changed the test protocol. We measured current amplitudes from the baseline before the treatment of calcium to the steady state current without MONNA and with MONNA over the concentration range of 1 nM to 100  $\mu$ M in the



MOL# 87502

presence of calcium (Fig. 5C). Concentration dependent block of ANO1 currents were obtained by measuring the % of remaining current and the  $IC_{50}$  was obtained from the dose-response curve (Fig. 5D). Although the  $IC_{50}$  for the slow current was slightly different from the  $IC_{50}$  for the fast current, MONNA still showed quite a high potency for blocking xANO1 ( $IC_{50\text{slow}} = 1.0 \mu\text{M}$ ).

To examine the reversibility of MONNA, we tested the washout of MONNA. Calcium-induced peak current of xANO1 fully recovered after treatment with  $0.1 \mu\text{M}$  MONNA (Fig. 5E). The percent of current amplitude after MONNA washing over current amplitude before MONNA treatment was  $98.2 \pm 3.4 \%$  (Fig. 5F).

### **MONNA is a selective blocker for ANO1**

The inhibitory effect of MONNA on other ion channels was evaluated to establish an ion channel selectivity profile for this derivative compound. To verify that MONNA also blocks other members of the ANO1 protein family, inhibitory activity was assessed on human ANO1 (hANO1) transiently expressed in HEK293 cells. hANO1 currents were measured by whole-cell patch-clamp recording in the presence of MONNA following 10 min pretreatment with MONNA at a range of concentrations ( $0.1 \sim 10 \mu\text{M}$ , Fig. 6A). The  $IC_{50}$  for MONNA in hANO1 was  $1.27 \mu\text{M}$ , as determined from the dose-response curve by measuring the current amplitude from  $+100 \text{ mV}$  to  $-100 \text{ mV}$  (Fig. 6B). There was no significant difference between the inward current and the outward current of hANO1 in terms of the block percentage (data not shown).

We further examined the blocking effect of MONNA on other chloride channels such as bestrophin-1, CLC2 and CFTR. For mouse bestrophin-1 (mBest1), endogenously expressed in cultured mouse cortical astrocytes ((Park et al., 2009), Fig. 6D), currents were recorded in the whole-cell patch-clamp mode with  $4.5 \mu\text{M Ca}^{2+}$  in the patch pipette. MONNA

MOL# 87502

(30  $\mu$ M) was treated 10 min before and during patching. HEK293 cells transiently transfected with cDNA of human bestrophin-1 (hBest1) or mouse CLC2 (mCLC2) were recorded with the whole-cell patch-clamp technique. HEK293 cells were held at 0 mV and stimulated with voltage steps ranging from  $-100$  to  $+100$  mV. Current amplitudes were collected before and 2-min after the application of 10  $\mu$ M MONNA. CFTR currents induced by isoproterenol were recorded with the two-electrode voltage-clamp method in *Xenopus laevis* oocytes co-injected with cRNA encoding human CFTR and the  $\beta$ -adrenergic receptor. The oocytes were held at  $-60$  mV and 10  $\mu$ M MONNA was added to the isoproterenol-containing solution (Fig. 6C). No significant blocking effect was observed with current responses in the presence of 30  $\mu$ M MONNA for mBest1 and 10  $\mu$ M MONNA for hBest1, mCLC2 and hCFTR (Fig. 6D).

## Discussion

In this study, we have identified a novel class of ANO1 blocker that inhibits the endogenous ANO1 in *Xenopus laevis* oocytes (xANO1), highlighting anthranilic acid derivatives with  $\beta$ -naphthyl possessing the substituent group  $-\text{OCH}_3$ ,  $-\text{I}$ , or  $-\text{Br}$ . Notably, *N*-((4-methoxy)-2-naphthyl)-5-nitroanthranilic acid (MONNA), an anthranilic derivative having  $\beta$ -naphthyl with a  $-\text{OCH}_3$  group at C10, is the most potent and selective blocker for xANO1 with an  $\text{IC}_{50}$  of 0.08  $\mu$ M.

Our drug screening method proved to be extremely efficient compared to the general blind screening for ion channel blockers. We validated the potent ANO1 blocker MONNA with less than 100 synthesized compounds. We were able to take advantage of target structure-focused libraries based on an anthranilic acid scaffold with specific substituents to arrive at the desired compounds because we are beginning with a lead compound that was a ANO1 blocker. Therefore, fewer compounds required screening in order to obtain hit

MOL# 87502

compounds. This strategy meant a smaller scale, higher quality screening process and dramatically reduced the subsequent hit-to lead timescale.

Currently available blockers for ANO1 must be applied in high concentrations to completely block ANO1 and are not very selective. Many attempts have been made to discover blockers for CaCCs; In particular, recent reports have focused on the high-throughput screening of small molecules that inhibit the activity of ANO1 (Huang et al., 2012; Namkung et al., 2011). Although these recently screened small molecule blockers have a high potency for ANO1 compared to conventional known blockers, selectivity profile of these blockers should follow.

The gating of Ano1 and the endogenous CaCC in oocytes is enigmatic and not completely understood (Kuruma and Hartzell, 2000; Xiao et al., 2011). However, all available evidence suggests that calcium-activated fast and slow currents are mediated by the same channel. Schroeder et al., showed that recording from an ionomycin-treated Axolotl oocytes injected with xANO1 cRNA had calcium-activated currents which had both fast and slow components (Schroeder et al., 2008). These two components with two distinct kinetics mediated by xANO1 channel are probably associated with different conformational states; the fast current is the open state and slow current may be a desensitized state. The conformational states of ion channels are believed to affect the affinity and efficacy of agonists and blockers. State-dependent affinity of ion channel blocker is a well-known phenomenon. Therefore, we can predict that different  $IC_{50}$ s of MONNA to the fast and slow currents of xANO1 come from the differential conformational states.

The profile of this new compound MONNA, as a selective blocker of ANO1, is very intriguing. MONNA strongly blocked chloride currents in xANO1 as well as in hANO1, suggesting a common blocking effect of MONNA in other members of the ANO1 protein family. The level of sensitivity in endogenous xANO1 was different from that of hANO1

MOL# 87502

expressed in HEK cells. In our previous report, we confirmed that untransfected HEK293 cells showed negligible  $\text{Ca}^{2+}$ -induced current response recorded in our condition (Park et al., 2009). Therefore, the difference of sensitivity for MONNA between endogenous xANO1 and hANO1 is not because of anion channel expression in HEK293 cells. Rather, differences in  $\text{IC}_{50}$  of MONNA between xANO1 and hANO1 possibly come from the conformational state or sequence or splice variant differences. To measure the blocking effect of MONNA to hANO1, current amplitude at one time point of 100 ~ 300 second after rupture was selected to be analyzed. We can predict that the conformational state of hANO1 is close to the desensitized state at this time point. Consistent with this idea,  $\text{IC}_{50}$  of hANO1 (1.27  $\mu\text{M}$ ) is not significantly different from the  $\text{IC}_{50\text{low}}$  of xANO1 (1.0  $\mu\text{M}$ ). The other possibility is the quantitative difference in pharmacology between over-expressed ANO1 and native CaCCs as previously reported (Oh et al., 2008; Yang et al., 2008). The concentration-current response from ANO1 channels over-expressed in HEK cells suggests a near complete block of currents by 10  $\mu\text{M}$  NFA, DIDS and NPPB (Yang et al., 2008), whereas NFA, DIDS and NPPB showed far less sensitivity to endogenous xANO1 with a  $\text{IC}_{50}$  of 37.3  $\mu\text{M}$ , 10.7  $\mu\text{M}$  and 32.3  $\mu\text{M}$  respectively, using our screening method (Oh et al., 2008). This is probably due to the molecular diversity within the ANO1 family or to splice variants of ANO1 which reflect the pharmacological diversity of the CaCC. Although whole-cell CaCC currents are superficially similar in different cell types including *Xenopus laevis* oocytes, various secretory epithelial cells, hepatocytes, vascular, airway and gut smooth muscle cells, Jurkat T-cells and pulmonary artery endothelial cells, there are significant differences in the pharmacology of these currents and their splice variants (Hartzell et al., 2005). Future studies to better understand the variable pharmacology of  $\text{Cl}^-$  channel-blocking drugs may include a determination of the specific expression of different members of the ANO1 family and ANO1 splice variants.

MOL# 87502

From our current results we are unable to distinguish whether the site of compound action on ANO1 is external or internal. However, a previous study revealed that diphenylamine-2-carboxylic acid (DPC) blocked from the outside and NFA blocked both from the inside and the outside when recordings were made in excised inside-out and outside-out patches from *Xenopus laevis* oocytes (Qu and Hartzell, 2001). There is a possibility that blocking of NFA from the inside involves NFA crossing the membrane in order to block from the outside. Because the molecular structure of MONNA is similar to that of DPC and NFA, we can predict that MONNA might also block xANO1 in a manner that is similar to DPC or NFA. There is a possibility that MONNA can bind to calcium binding site of ANO1 from the inside of the cells and to influence the calcium dependence of ANO1. The crystal structure of ANO1 is not fully known, but when such structural information becomes available, the drug discovery process should be significantly accelerated. Meanwhile, the availability of a selective blocker for ANO1 should be beneficial for further understanding the function of ANO1 and for possible therapeutic applications in those diseases associated with ANO1.

### **Authorship Contributions**

*Participated in research design:* Oh, Hwang, Hartzell, Roh and Lee.

*Conducted experiments:* Oh, Hwang, Jung, Yu, Kim and Choi.

*Contributed new reagents or analytic tools:* Oh, Hwang, Jung and Roh.

*Performed data analysis:* Oh, Hwang, Jung, Yu, Kim, Hartzell, Roh and Lee.

*Wrote or contributed to the writing of the manuscript:* Oh, Hwang, Yu, Hartzell, Roh and Lee.

MOL# 87502

## References

- Barish ME (1983) A transient calcium-dependent chloride current in the immature *Xenopus* oocyte. *J Physiol* **342**: 309-325.
- Caputo A, Caci E, Ferrera L, Pedemonte N, Barsanti C, Sondo E, Pfeiffer U, Ravazzolo R, Zegarra-Moran O and Galiotta LJ (2008) TMEM16A, a membrane protein associated with calcium-dependent chloride channel activity. *Science* **322**(5901): 590-594.
- Cho H, Yang YD, Lee J, Lee B, Kim T, Jang Y, Back SK, Na HS, Harfe BD, Wang F, Raouf R, Wood JN and Oh U (2012) The calcium-activated chloride channel anoctamin 1 acts as a heat sensor in nociceptive neurons. *Nat Neurosci* **15**(7): 1015-1021.
- Greenwood IA and Large WA (1998) Properties of a Cl<sup>-</sup> current activated by cell swelling in rabbit portal vein vascular smooth muscle cells. *Am J Physiol* **275**(5 Pt 2): H1524-1532.
- Greenwood IA and Leblanc N (2007) Overlapping pharmacology of Ca<sup>2+</sup>-activated Cl<sup>-</sup> and K<sup>+</sup> channels. *Trends Pharmacol Sci* **28**(1): 1-5.
- Hartzell C, Putzier I and Arreola J (2005) Calcium-activated chloride channels. *Annu Rev Physiol* **67**: 719-758.
- Huang F, Rock JR, Harfe BD, Cheng T, Huang X, Jan YN and Jan LY (2009) Studies on expression and function of the TMEM16A calcium-activated chloride channel. *Proceedings of the National Academy of Sciences of the United States of America* **106**(50): 21413-21418.
- Huang F, Zhang H, Wu M, Yang H, Kudo M, Peters CJ, Woodruff PG, Solberg OD, Donne ML, Huang X, Sheppard D, Fahy JV, Wolters PJ, Hogan BL, Finkbeiner WE, Li M, Jan YN, Jan LY and Rock JR (2012) Calcium-activated chloride channel TMEM16A modulates mucin secretion and airway smooth muscle contraction. *Proceedings of the National Academy of Sciences of the United States of America* **109**(40): 16354-16359.
- Kuruma A and Hartzell HC (2000) Bimodal control of a Ca(2+)-activated Cl(-) channel by different Ca(2+) signals. *The Journal of general physiology* **115**(1): 59-80.
- Miledi R (1982) A calcium-dependent transient outward current in *Xenopus laevis* oocytes. *Proc R Soc Lond B Biol Sci* **215**(1201): 491-497.
- Namkung W, Phuan PW and Verkman AS (2011) TMEM16A inhibitors reveal TMEM16A as a minor component of calcium-activated chloride channel conductance in airway and intestinal epithelial cells. *J Biol Chem* **286**(3): 2365-2374.
- Oh SJ, Park JH, Han S, Lee JK, Roh EJ and Lee CJ (2008) Development of selective blockers for Ca(2+)-activated Cl channel using *Xenopus laevis* oocytes with an improved drug screening strategy. *Mol Brain* **1**: 14.
- Park H, Oh SJ, Han KS, Woo DH, Park H, Mannaioni G, Traynelis SF and Lee CJ (2009) Bestrophin-1 encodes for the Ca<sup>2+</sup>-activated anion channel in hippocampal astrocytes. *J Neurosci* **29**(41): 13063-13073.
- Qu Z and Hartzell HC (2001) Functional geometry of the permeation pathway of Ca<sup>2+</sup>-activated Cl-channels inferred from analysis of voltage-dependent block. *J Biol Chem* **276**(21): 18423-18429.
- Reinsprecht M, Rohn MH, Spadinger RJ, Pecht I, Schindler H and Romanin C (1995) Blockade of capacitive Ca<sup>2+</sup> influx by Cl<sup>-</sup> channel blockers inhibits secretion from rat mucosal-type mast cells. *Mol Pharmacol* **47**(5): 1014-1020.
- Schroeder BC, Cheng T, Jan YN and Jan LY (2008) Expression cloning of TMEM16A as a calcium-activated chloride channel subunit. *Cell* **134**(6): 1019-1029.

MOL# 87502

- Schultheiss G, Frings M, Hollingshaus G and Diener M (2000) Multiple action sites of flufenamate on ion transport across the rat distal colon. *Br J Pharmacol* **130**(4): 875-885.
- Shaw T, Lee RJ and Partridge LD (1995) Action of diphenylamine carboxylate derivatives, a family of non-steroidal anti-inflammatory drugs, on  $[Ca^{2+}]_i$  and  $Ca^{2+}$ -activated channels in neurons. *Neurosci Lett* **190**(2): 121-124.
- Verkman AS and Galiotta LJ (2009) Chloride channels as drug targets. *Nat Rev Drug Discov* **8**(2): 153-171.
- Wang HS, Dixon JE and McKinnon D (1997) Unexpected and differential effects of Cl<sup>-</sup> channel blockers on the Kv4.3 and Kv4.2 K<sup>+</sup> channels. Implications for the study of the I(to2) current. *Circ Res* **81**(5): 711-718.
- Xiao Q, Yu K, Perez-Cornejo P, Cui Y, Arreola J and Hartzell HC (2011) Voltage- and calcium-dependent gating of TMEM16A/Ano1 chloride channels are physically coupled by the first intracellular loop. *Proceedings of the National Academy of Sciences of the United States of America* **108**(21): 8891-8896.
- Xu WX, Kim SJ, So I, Kang TM, Rhee JC and Kim KW (1997) Volume-sensitive chloride current activated by hyposmotic swelling in antral gastric myocytes of the guinea-pig. *Pflugers Arch* **435**(1): 9-19.
- Yang YD, Cho H, Koo JY, Tak MH, Cho Y, Shim WS, Park SP, Lee J, Lee B, Kim BM, Raouf R, Shin YK and Oh U (2008) TMEM16A confers receptor-activated calcium-dependent chloride conductance. *Nature* **455**(7217): 1210-1215.

MOL# 87502

## Footnotes

S-J.O and S.J.H contributed equally to this work.

C.J.L. and E.J.R. contributed equally to this work.

This work was supported by the KIST Institutional Program [Grant 2E24182], the World Class Institute (WCI) Program of the National Research Foundation of Korea (NRF) funded by the Ministry of Education, Science and Technology of Korea [Grant WCI 2009-003], NIH grants [GM60448] and [EY11482] and a pilot grant from the Emory Center for Cystic Fibrosis Research of Children's Healthcare of Atlanta.



MOL# 87502

## Legends for figures

Fig. 1. General synthesis procedures

Reagents and conditions. Step A. TMSCl (trimethylsilyl chloride), MeOH, reflux; Step B. OTf<sub>2</sub>, pyridine, DCM (dichloromethane), -78 °C to room temperature; Step C. BINAP (2,2'-bis(diphenylphosphino)-1,1'-naphthyl), Pd<sub>2</sub>(dba)<sub>3</sub>·CHCl<sub>3</sub> (Tris(dibenzylideneacetone)dipalladium-chloroform adduct), CsCO<sub>3</sub>, toluene, 110 ~ 130 °C; Step D. Cul, NaI, *trans*-N,N'-dimethylcyclohexane-1,2-diamine, 1,4-dioxane, 110 °C; Step E. LiOH, THF/MeOH/H<sub>2</sub>O (5 : 3 : 2), reflux.

Fig. 2. Potency of synthesized derivatives with a phenyl group at the B position.

A. Representative trace of xANO1 currents induced by 4-repetitive 5 mM calcium treatments.

B. Summary of the experiments shown in A. Bar graph shows the stable currents with almost the same amplitude induced by 4-repetitive calcium treatments. Amplitude of second, third and fourth current was normalized by the amplitude of first current respectively (n = 7). Error bars indicate SEMs.

C. Representative traces of xANO1 currents by simultaneous 4-channel recording before and during application of N-(4-trifluorophenyl)-4-nitroanthranilic acid (4TFP4NA). Oocytes were pre-incubated with 4TFP4NA for 30 s and currents were induced by 5 s applications of extracellular Ca<sup>2+</sup>. The currents were measured at -60 mV.

D. Representative dose-response relation of 4TFP4NA block of xANO1 currents (n = 8). Error bars indicate SEMs.

E. Structure of synthesized compound.

MOL# 87502

F. Summary table for substituents and the  $IC_{50}$  of tested compounds. Position A2 showed the most potent blocking effect. Comp. indicates compounds described in Fig. 1, which shows the synthesis procedures.

Fig. 3.  $-NO_2$  at A2 of benzoic acid ring with phenyl ring substituted anthranilic acid and  $-NO_2$  at A1 of benzoic acid with naphthyl group substituted anthranilic acid showed the higher potencies.

A. Structure of synthesized compound.

B. Summary table for substituents and the  $IC_{50}$  of tested compounds.  $-NO_2$  at position A2 has a better blocking effect than  $-CF_3$ .

C. Summary table for substituents and the  $IC_{50}$  of tested compounds.  $-NO_2$  at position A2 is best for the phenyl ring, and at position A1 is best for naphthyl.

Fig. 4. Effect of substituent position in the naphthyl group on blocking potency.

A and C. Structure of synthesized compound.

B, D and E. Summary table for substituents and the  $IC_{50}$  of tested compounds.  $-OCH_3$  at position C10 of  $\beta$ -naphthyl has the most potent blocking effect.

Fig. 5. Validation of potent blocker MONNA on the steady state current

A. Representative traces to show blocking of  $Ba^{2+}$ -induced currents by MONNA and 4TFMPA in ionophore. The current was measured at  $-60$  mV.

B. Structure of tested compounds and summary bar graph of the experiments shown in A. Each number in the bar indicates the number of cells tested. Error bars indicate SEMs. n.s means no significant statistical difference with the 2-tailed t-test.

MOL# 87502

C. Representative traces for test blocking effect of MONNA on the slow steady current component. A dashed line indicates the baseline. Current amplitudes were measured from baseline before the treatment of calcium to the steady state current without MONNA and with MONNA over the concentration range in the presence of calcium.

D.  $IC_{50}$  and dose-response relation of MONNA for the slow current component of the  $Ca^{2+}$ -activated  $Cl^{-}$  current. Concentration dependent block of ANO1 currents were obtained by measuring the % of remaining current and  $IC_{50}$  was obtained from the dose-response curves.

E. Representative trace to show the washout of MONNA. 0.1  $\mu M$  MONNA was fully washed out after 100 s wash with recording solution.

F. Summary bar graph of % current amplitude measured from the experiments shown in E ( $n = 9$ ). Error bars indicate SEMs. n.s means no significant difference by means no significant statistical difference with the 2-tailed t-test.

Fig. 6. MONNA is a selective blocker for ANO1

A. Representative I-V response of HEK293 cells expressing hANO1 under the whole-cell patch-clamp configuration, with 4.5  $\mu M$   $Ca^{2+}$  in the patch pipette. Each current trace was normalized to the current measured at +100 mV.

B.  $IC_{50}$  and dose-response relation of MONNA for hANO1 ( $n = 3 \sim 12$ ).

C. Representative trace to show the effect of MONNA on the hCFTR currents induced by treatment with 10  $\mu M$  isoproterenol in voltage-clamped *Xenopus laevis* oocytes expressing hCFTR and the  $\beta$ -adrenergic receptor.

D. Bar graph to show the blocking effect of MONNA on other chloride channels. Responses to various chloride channels were evaluated in cultured mouse cortical astrocytes expressing endogenous mBest1 or in transiently transfected HEK293 cells expressing hBest1 or mCLC2,

MOL# 87502

or in *Xenopus laevis* oocytes stably expressing hCFTR, in the absence or presence of MONNA. 30  $\mu$ M MONNA was applied to cells expressing mBest1, 10  $\mu$ M MONNA was applied to hBest1, mCLC2 and hCFTR. Each number in the bar indicates the number of cells tested. Error bars indicate SEMs.

Figure 1

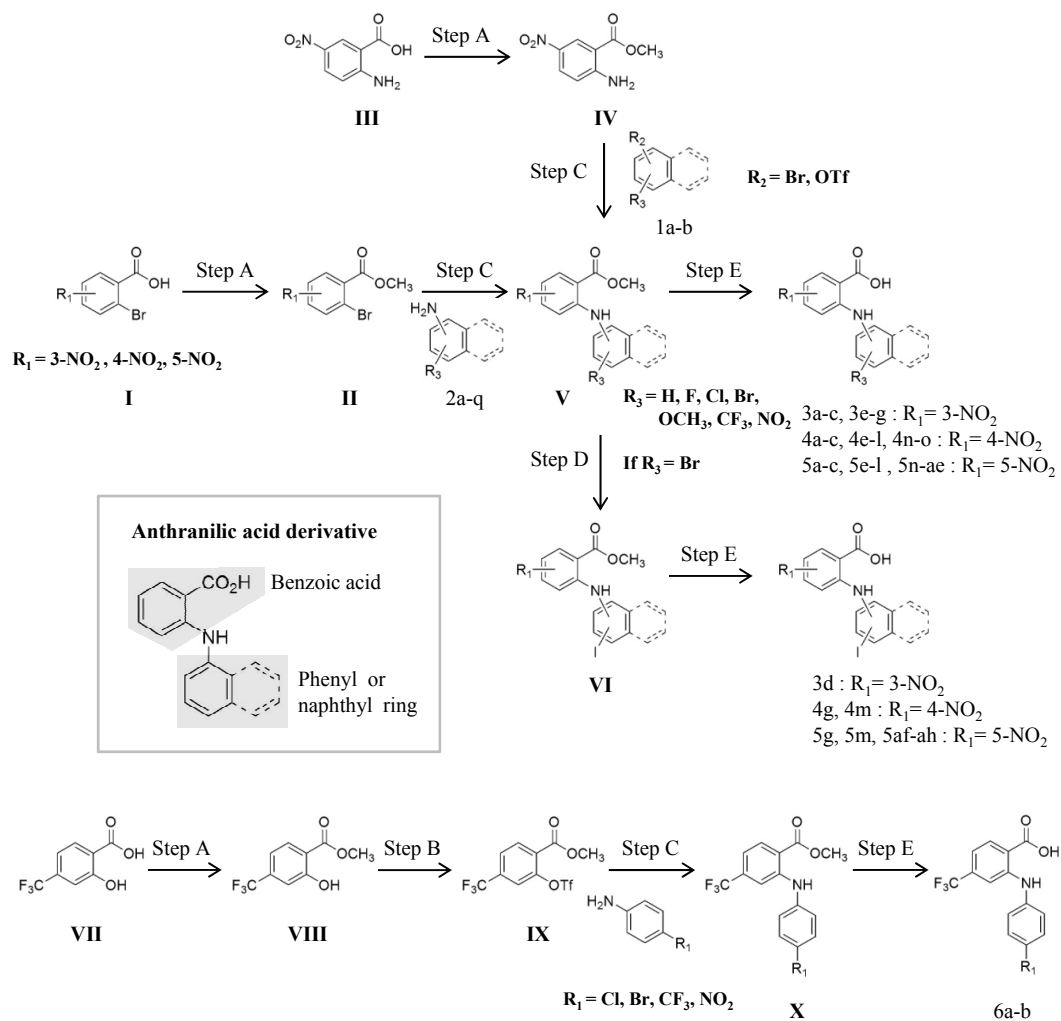


## Figure 2

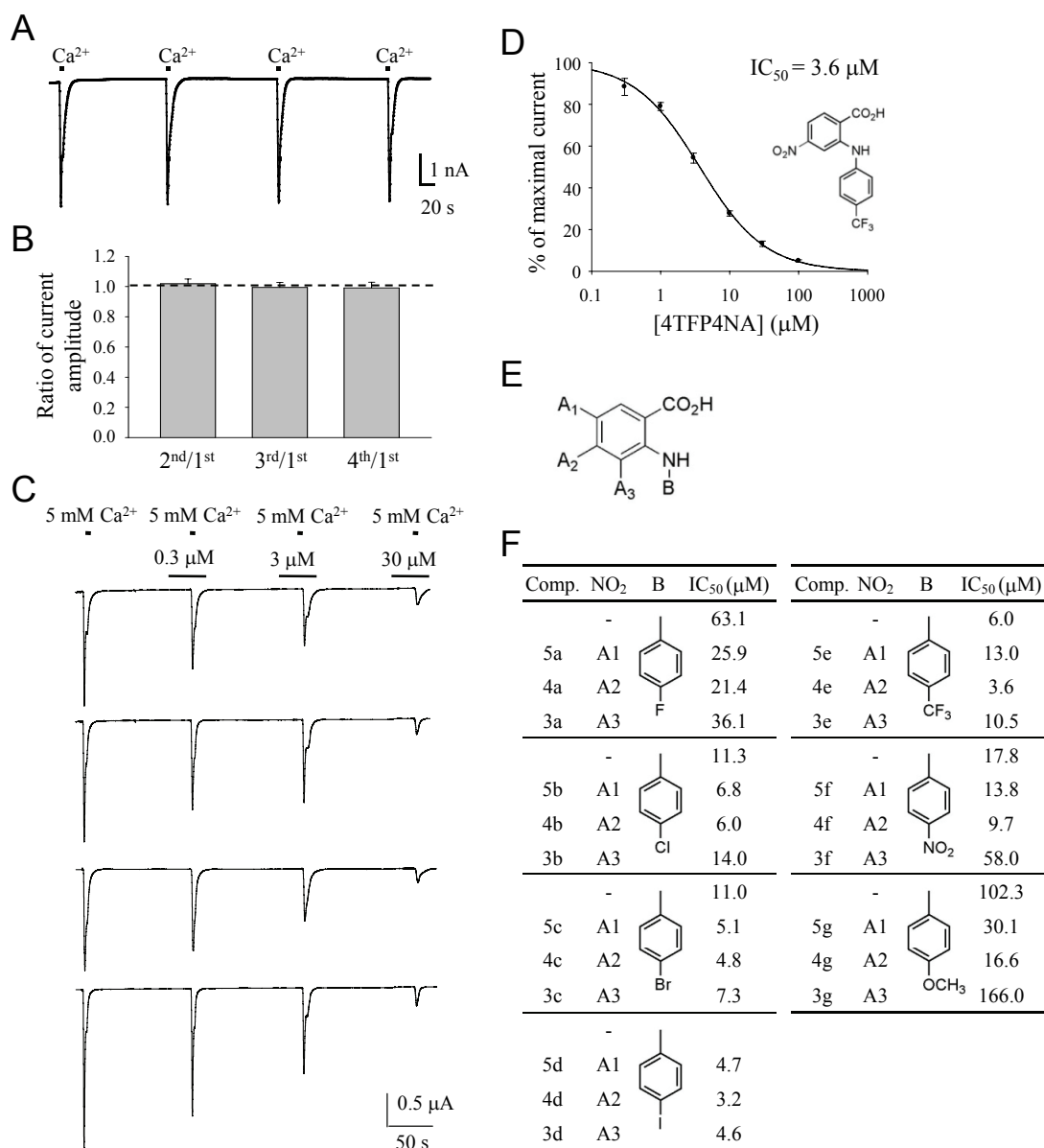
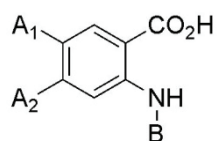


## Figure 3

A



B

Comp.	A2	B	IC <sub>50</sub> (μM)
4b	NO <sub>2</sub>		6.0
6a	CF <sub>3</sub>		10.2
4c	NO <sub>2</sub>		4.8
6b	CF <sub>3</sub>		16.1
4f	NO <sub>2</sub>		9.7
6c	CF <sub>3</sub>		34.5
4e	NO <sub>2</sub>		3.6
6d	CF <sub>3</sub>		19.8

C

Comp.	NO <sub>2</sub>	B	IC <sub>50</sub> (μM)	Comp.	NO <sub>2</sub>	B	IC <sub>50</sub> (μM)
5h	A1		42.5	5i	A1		5.0
4h	A2		28.3	4i	A2		8.5
5a	A1		25.9	5j	A1		3.0
4a	A2		21.4	4j	A2		13.6
5b	A1		6.8	5k	A1		Insoluble
4b	A2		6.0	4k	A2		3.8
5c	A1		5.1	5l	A1		1.5
4c	A2		4.8	4l	A2		10.1
5d	A1		4.7	5m	A1		1.2
4d	A2		3.2	4m	A2		17.1
5f	A1		13.8	5n	A1		
4f	A2		9.7	4n	A2		21.6
5g	A1		30.1	5o	A1		2.3
4g	A2		16.6	4o	A2		15.7

Figure 4

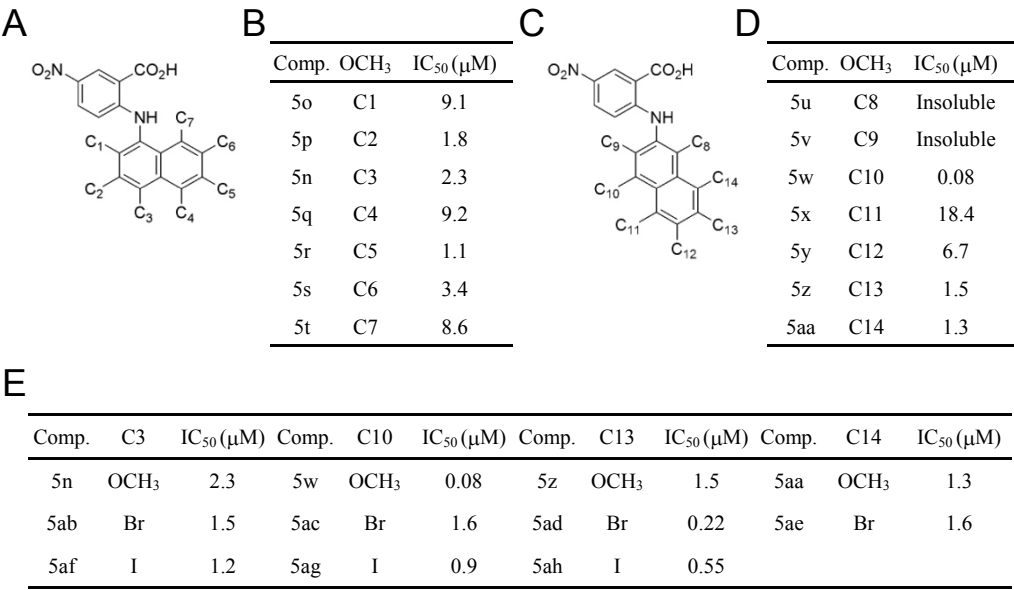




## Figure 5

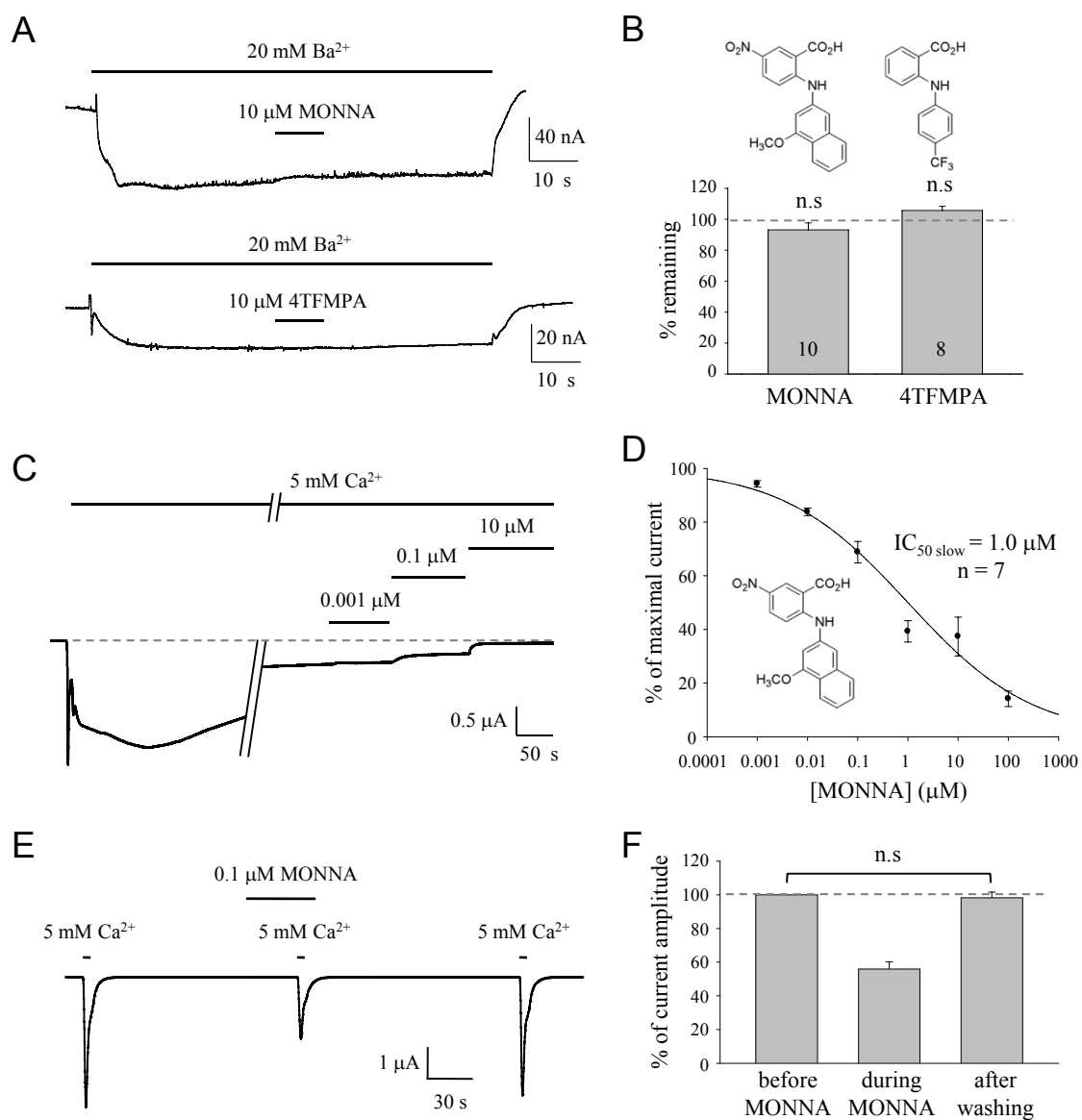


Figure 6

